Year: 2022

MALDI mass spectrometry imaging - Diagnostic pathways and metabolites for renal tumor entities

Erlmeier, Franziska ; Sun, Na ; Shen, Jian-Ren ; Feuchtinger, Annette ; Buck, Achim ; Prade, Verena M ; Kunzke, Thomas ; Schraml, Peter ; Moch, Holger ; Autenrieth, Michael ; Weichert, Wilko ; Hartmann, Arndt ; Walch, Axel

Abstract: BACKGROUND Correct tumor subtyping of primary renal tumors is essential for treatment decision in daily routine. Most of the tumors can be classified on morphology alone. Nevertheless, some diagnoses are difficult and further investigations are needed for correct tumor subtyping. Beside histochemical investigations high mass resolution matrix-assisted laser desorption/ionization mass spectrometry imaging (MALDI-MSI) can detect new diagnostic biomarkers and hence improve the diagnostic. PATIENTS AND METHODS Formalin-fixed paraffin embedded (FFPE) tissue specimens from clear cell renal cell carcinoma (ccRCC, n=552), papillary RCC (pRCC, n=122), chromophobe RCC (chRCC, n=108) and renal Oncocytoma (rO, n=71) were analyzed by high mass resolution matrix-assisted laser desorption/ionization (MALDI) fourier-transform ion cyclotron resonance (FT-ICR) mass spectrometry imaging (MSI). SPACiAL pipeline was executed for automated co-registration of histological and molecular features. Pathway enrichment and pathway topology analysis were performed to determine significant differences between RCC subtypes. RESULTS We discriminated the four histological subtypes (ccRCC, pRCC, chRCC and rO) and established the subtype specific pathways and metabolic profiles. RO showed an enrichment of pentose phosphate, taurine and hypotaurine, glycerophospholipid, amino sugar and nucleotide sugar, fructose and mannose, glycine, serine and threonine pathways. ChRCC is defined by enriched pathways including the amino sugar and nucleotide sugar, fructose and mannose, glycerophospholipid, taurine and hypotaurine, glycine, serine and threonine pathways. Pyrimidine, amino sugar and nucleotide sugar, glycerophospholipid and glutathione pathways are enriched in ccRCC. Furthermore, we detected enriched phosphatidylinositol and glycerophospholipid pathways in pRCC. CONCLUSION In summary, we performed a classification system with a mean accuracy in tumor discrimination of 85,13%. Furthermore, we detected tumor specific biomarkers for the four most common primary renal tumors by MALDI-MSI. This method is a useful tool in differential diagnosis and in biomarker detection.

Originally published at:
Erlmeier, Franziska; Sun, Na; Shen, Jian-Ren; Feuchtinger, Annette; Buck, Achim; Prade, Verena M; Kunzke, Thomas; Schraml, Peter; Moch, Holger; Autenrieth, Michael; Weichert, Wilko; Hartmann,

Oncology

MALDI mass spectrometry imaging - Diagnostic pathways and metabolites for renal tumor entities

Erlmeier F, Sun N, Shen J, Feuchtinger A, Buck A, Prade VM, Kunzke T, Schraml P, Moch H, Autenrieth M, Weichert W, Hartmann A, Walch A

Disclaimer:
Accepted, unedited article not yet assigned to an issue. The statements, opinions and data contained in this publication are solely those of the individual authors and contributors and not of the publisher and the editor(s). The publisher and the editor(s) disclaim responsibility for any injury to persons or property resulting from any ideas, methods, instructions or products referred to the content.

MALDI mass spectrometry imaging - Diagnostic pathways and metabolites for renal tumor entities

Franziska Erlmeier[1*], Na Sun[2*], Jian Shen[2], Annette Feuchtinger[2], Achim Buck[2], Verena M. Prade[2], Thomas Kunzke[2], Peter Schraml[3], Holger Moch[3], Michael Autenrieth[4], Wilko Weichert[5], Arndt Hartmann[1], Axel Walch[2]

[1]Institute of Pathology, University Hospital Erlangen-Nuernberg, Erlangen, Germany
[2]Research Unit Analytical Pathology, Helmholtz Zentrum München – German Research Center for Environmental Health, Neuherberg, Germany
[3] Department of Pathology and Molecular Pathology, University Hospital Zurich, Zurich, Switzerland
[4] Department of Urology, Rechts der Isar Medical Center, Technical University of Munich, Munich, Germany
[5] Institute of Pathology, Technical University Munich, Munich, Germany
* contributed equally to this work

Corresponding author:

Franziska Erlmeier, MD
Institute of Pathology
University Hospital Erlangen-Nuernberg
Friedrich Alexander University (FAU)
91054 Erlangen, Germany
Phone: +49 9131 85 22286
Email: f.erlmeier@icloud.com

Abstract
Background: Correct tumor subtyping of primary renal tumors is essential for treatment decision in daily routine. Most of the tumors can be classified on morphology alone. Nevertheless, some diagnoses are difficult and further investigations are needed for correct tumor subtyping. Beside histochemical investigations high mass resolution

matrix-assisted laser desorption/ionization mass spectrometry imaging (MALDI-MSI) can detect new diagnostic biomarkers and hence improve the diagnostic.

Patients and Methods: Formalin-fixed paraffin embedded (FFPE) tissue specimens from clear cell renal cell carcinoma (ccRCC, n=552), papillary RCC (pRCC, n=122), chromophobe RCC (chRCC, n=108) and renal Oncocytoma (rO, n=71) were analyzed by high mass resolution matrix-assisted laser desorption/ionization (MALDI) fourier-transform ion cyclotron resonance (FT-ICR) mass spectrometry imaging (MSI). SPACiAL pipeline was executed for automated co-registration of histological and molecular features. Pathway enrichment and pathway topology analysis were performed to determine significant differences between RCC subtypes.

Results: We discriminated the four histological subtypes (ccRCC, pRCC, chRCC and rO) and established the subtype specific pathways and metabolic profiles. RO showed an enrichment of pentose phosphate, taurine and hypotaurine, glycerophospholipid, amino sugar and nucleotide sugar, fructose and mannose, glycine, serine and threonine pathways. ChRCC is defined by enriched pathways including the amino sugar and nucleotide sugar, fructose and mannose, glycerophospholipid, taurine and hypotaurine, glycine, serine and threonine pathways. Pyrimidine, amino sugar and nucleotide sugar, glycerophospholipid and glutathione pathways are enriched in ccRCC. Furthermore, we detected enriched phosphatidylinositol and glycerophospholipid pathways in pRCC.

Conclusion: In summary, we performed a classification system with a mean accuracy in tumor discrimination of 85,13%. Furthermore, we detected tumor specific biomarkers for the four most common primary renal tumors by MALDI-MSI. This method is a useful tool in differential diagnosis and in biomarker detection.

Abbreviations:
[109]AgNPET LDI MS   laser desorption/ionization mass spectrometry
ATP   adenosin triphosphate
ccRCC   clear cell renal cell carcinoma
chRCC   chromophobe renal cell carcinoma
CK7   cytokeratin 7
CSS   cancer specific survival
FFPE   formalin fixed paraffin embedded
FT-ICR   fourier-transform ion cyclotron resonance
G-Met   global metabolomics
^{1}H NMR   high-resolution proton nuclear magnetic resonance spectroscopy
MALDI   high mass resolution matrix-assisted laser desorption/ionization
MSI   mass spectrometry imaging

pRCC	papillary renal cell carcinoma
PFS	progression free survival
rO	renal oncocytoma
TMA	tissue microarray

Introduction

Tumor subtyping of primary renal tumors is essential and daily work in routine histopathological diagnostic. The most common subtypes of primary renal tumors are the clear cell renal cell carcinoma (ccRCC), the papillary renal cell carcinoma (pRCC), the chromophobe renal cell carcinoma (chRCC) and the renal oncocytoma (rO)[1, 2]. Most of these tumors can be diagnosed with morphology alone. In difficult cases further investigations, such as immunohistochemical or molecular analysis, are needed. The ccRCC shows a typical histopathology with solid alveolar and acinar patterns. The tumor typically contains a network of thinwalled blood vessels. The cells have a clear cytoplasm surrounded by distinct cell membranes. The pRCC typically show a papillary architecture. They contain papillae formed by delicate fibrovascular cores. These tumors usually do not cause any diagnostic problems. However, the differential diagnosis of oncocytic renal tumors can be very challenging. Oncocytic tumors include inter alia the oncocytic pRCC, the chRCC and the rO. All of these tumors show a partly eosinophilic finely granular cytoplasm. The oncocytic pRCC contain voluminous, finely granular, distributed eosinophilic cytoplasm. The nucleolar grade is usually low with uniform round nuclei [1]. In the chRCC typically a solid sheet-like pattern can be found with two mixed cell types. On the one hand, you can find pale cells with a prominent cell border. On the other hand, the eosinophilic type of chRCC contain smaller cells with finely granulated, eosinophilic cytoplasm. Renal Oncocytomas show a solid nested architecture with small islands of oncocytic cells. To discriminate oncocytic tumors the mostly used method is immunohistochemistry [3, 4]. Therefore, Cytokeratin 7 (CK7) is a useful marker. ChRCC often show a positive staining rection, which may be focal in eosinophilic cells. Whereas, rO is usually negative for CK7. In some case single focally positive cells can be found [5, 6]. In pRCC a positive CK7 reaction is more common in type 1 tumors. Another investigation for tumor subtyping is the colloidal iron staining, also called Hale staining. ChRCC show an intense reticular staining pattern. This staining method often causes trouble because of its difficult standardization. This leads to an interobserver variability in routine diagnostic.

Up to now, some cases of primary renal tumors cause problems in routine histopathology. New diagnostic biomarkers could help to improve the renal tumor subtyping. Several studies demonstrated that mass spectrometry imaging (MSI) is a useful tool to discriminate between renal tumor subtypes [7, 8]. In our study we analyzed a multicenter cohort including 853 primary renal tumors with four histological subtypes by high mass resolution matrix-assisted laser desorption/ionization mass spectrometry imaging (MALDI-MSI). We discriminated the four histological subtypes and established the subtype specific metabolites.

Materials and Methods

Patient tissues

Formalin fixed paraffin embedded (FFPE) renal tumor samples comprising 552 clear cell renal cell carcinoma (ccRCC), 122 papillary renal cell carcinoma (pRCC), 108 chromophobe renal cell carcinoma (chRCC) and 71 renal oncocytoma (RO) were collected from the archives of the Department of Pathology and Molecular Pathology of the University Hospital Zurich (1993-2013) and of the Technical University of Munich (1996-2014). Tissue microarrays (TMAs) were constructed as described [9].Tissue cylinders with 0.6 mm (Zurich) and 1.0 mm (Munich) diameter were punched from morphologically representative regions of paraffin donor blocks. The samples were collected in close collaboration with the local departments of urology.

MALDI mass spectrometry imaging

Tissue preparation steps for the high mass resolution matrix-assisted laser desorption/ionization (MALDI) fourier-transform ion cyclotron resonance (FT-ICR) mass spectrometry imaging analysis was performed as previously described [10]. In brief, FFPE TMAs were sectioned with 4 μm (Microm, HM340E, Thermo Fisher Scientific, USA) and mounted onto indium-tin-oxide (ITO)-coated glass slides (Bruker Daltonik, Bremen, Germany) pretreated with 1:1 poly-L-lysine (Sigma Aldrich, Munich, Germany) and 0.1% Nonidet P-40 (Sigma-Aldrich, Munich, Germany). FFPE sections were incubated for 1 h at 70°C, deparaffinized in xylene (2 x 8 min), and air-dried. The matrix solution consisted of 10 mg/ml 9-aminoacridine hydrochloride monohydrate (9-AA) (Sigma-Aldrich, Germany) in water/methanol 30:70 (v/v). Spray-coating of the matrix was conducted using the SunCollectTM sprayer (Sunchrom, Friedrichsdorf, Germany) in eight passes (10 μl/min, 20 μl/min, 30 μl/min for layers 1-3, and layers 4-8 with 40 μl/min), utilizing 2 mm line distance and a spray velocity of 900 mm/min.

Metabolites were detected in negative-ion mode on a 7 T Solarix XR FT-ICR mass spectrometer (Bruker Daltonik) equipped with a dual ESI-MALDI source and a SmartBeam-II Nd: YAG (355 nm) laser. Mass spectra were acquired in negative-ion mode covering m/z 75-1000. For internal mass calibration, the 9-AA matrix ion signal (m/z 193.0771) was used as lock mass minimizing scan-to-scan (pixel-to-pixel) variations during the MALDI measurement. The laser operated at a frequency of 1,000 Hz utilizing 200 laser shots per pixel with a pixel resolution of 60 μm. External calibration of the instrument was performed with L-Arginine in the ESI mode. MALDI mass spectra were root mean square normalized with SCiLS (v. 2020b Pro) and picked peaks were exported as imzML files for further data processing and subsequent analysis with the SPACiAL pipeline. Peak annotation was performed using HMDB (http://www.hmdb.ca/)[11] and METASPACE (http://annotate.metaspace2020.eu/)[12] databases, while allowing M-H, M-H2O, M+K-2H, M+Na-2H, and M+Cl as negative adducts with a mass tolerance of 4 ppm (Ion mode: negative, Adduct type: (M-H), (M-H-H2O), (M+Na-2H), (M+Cl) and (M+K-2H), mass accuracy≤4 ppm). Pathway enrichment analysis was performed with the MetaboAnalyst (http://www.metaboanalyst.ca) [13] and Kyoto Encyclopedia of Genes and Genomes (KEGG) database (http://www.genome.jp/kegg/) [14]. Briefly, algorithms including hypergeometric test for over representation analysis and relative-betweeness centrality for pathway topology analysis were selected. Homo sapiens (KEGG) were specified as pathway library. The metabolome view was generated according to the p values from the pathway enrichment analysis and pathway impact values from the pathway topology analysis. Kruskal-Wallis test with subsequent Benjamini-Hochberg correction were performed to determine significant differences between RCC subtypes.

Results:

Sample description and MALDI-MSI experiments

Spatial metabolomic was performed for renal carcinoma tissue sections from 853 patients comprising four tumor subtypes - clear cell renal cell carcinomas (ccRCC, n = 552), papillary renal cell carcinomas (pRCC, n = 122), chromophobe renal cell carcinomas (chRCC, n = 108) and renal oncocytomas (RO, n = 71) (Table 1). The workflow integrated high mass resolution matrix-assisted laser desorption/ionization (MALDI) fourier-transform ion cyclotron resonance (FT-ICR) mass spectrometry imaging (MSI) analysis, SPACiAL pipeline for automated co-registration of histological and molecular features, bioinformatics analysis for pathway-specific phenotyping and patient diagnosis analysis (Figure 1).

Within the mass range of *m/z* 75 to 1000, in total 2111 metabolite peaks were resolved. These metabolic features were used for further statistic and prognosis analysis.

MALDI-MSI workflow started with matrix application on tissue sections, mass spectra processing and visual MS images generation. The matrix was then removed for subsequent H&E staining of the very same tissue section. The H&E images were precisely co-registered to the coordinates of the mass spectra per pixel. The SPACiAL pipeline automatically integrated molecular MALDI-MS data with histological staining data. After data extraction, pathway enrichment analysis and statistical analysis were performed.

Pathway enrichment analysis

For pathway enrichment analysis, the MS spectrum of tumor regions of individual patients was compared between different renal tumor subtypes. Masses with a peak intensity 1.5 -fold higher than the average spectrum were defined as discriminative masses of the corresponding renal tumor subtype. The discriminative masses of each subtype were then annotated in metabolite databases (HMDB and METASPACE). Pathway enrichment analyses were performed with MetaboAnalyst 5.0. As a result, enriched metabolic pathways contributed to subtype discrimination including pentose phosphate, taurine and hypotaurine, glycerophospholipid, amino sugar and nucleotide sugar, fructose and mannose, glycine, serine and threonine pathways for RO; amino sugar and nucleotide sugar, fructose and mannose, glycerophospholipid, taurine and hypotaurine, glycine, serine and threonine pathways for chRCC; pyrimidine, amino sugar and nucleotide sugar, glycerophospholipid and glutathione pathways for ccRCC; and phosphatidylinositol, glycerophospholipid pathways for pRCC (Figure 2).

Pathway enrichment analysis was performed using MetaboAnalyst 5.0 (http://www.metaboanalyst.ca). Metabolic pathways were represented as circles according to their scores from enrichment (vertical axis) and topology analyses (pathway impact, horizontal axis). The color of circles indicated the statistical significance of the overall metabolic changes within the pathway and circle diameter represented the relative impact of differential metabolites within the pathway as indicated. The discriminative pathways of renal tumor subtypes were indicated in the figure.

We provided example ion images of the metabolites, which showed significant differences between the RCC subtypes (Figure 3). As a result, heterogeneous histological distributions and significant differences abundances of the example metabolites could be observed in different subtypes of RCC. Ribose 5-phosphate from pentose phosphate pathway

was mostly abundant in rO. Glucosamine from amino sugar and nucleotide sugar metabolism pathway was dominantly abundant in rO and chRCC. Uridine 5'-diphosphate from pyrimidine metabolism pathway represented higher abundancy in rO, chRCC and ccRCC compared with pRCC. Conversely, 3-dehyrocarnitine was highly abundant in ccRCC and pRCC, however represented the lowest abundancy in rO.

Discussion

The correct tumor classification is essential for appropriate patient treatment. In the majority of cases the tumor can be classified by histological investigation alone. Especially the subtyping of oncocytic tumors needs further investigations, such as immunohistochemistry or molecular analysis. Several studies already demonstrated the diagnostic power of mass spectrometry imaging. Zhang et al. analyzed 81 frozen human tissue samples including normal kidney, rO and several RCC subtypes. They achieved an overall accuracy of 99,47% for tissue discrimination [15]. Furthermore, Kriegsmann et al. analyzed 135 chRCC and rO patient tissues by MSI and they achieved a median accuracy of 89% [8]. Therefore, MSI is an appropriate tool to discriminate tumor subtypes and to detect novel potential diagnostic pathways.

Our results defined several metabolic pathways and metabolites, which are enriched in special tumor subtypes. The mean accuracy in tumor discrimination was 85,13%. RO showed an enrichment of pentose phosphate, taurine and hypotaurine, glycerophospholipid, amino sugar and nucleotide sugar, fructose and mannose, glycine, serine and threonine pathways. Moreover, Ribose 5-phosphate from pentose phosphate pathway was mostly abundant in rO. The pentose phosphate pathway is an alternative metabolic pathway which generates precursors for nucleotide biosynthesis and NADPH for anabolic reactions and redox homeostasis maintenance [16, 17]. The pathway starts with glucose-6-phosphate, which plays a central role in ccRCC [18]. Lucarelli et al. suggested that ccRCC patients with high levels of glycolytic enzymes showed a reduced progression free survival (PFS) and cancer specific survival (CSS). The role of this pathway in rO remains unclear.

ChRCC is defined by enriched pathways including the amino sugar and nucleotide sugar, fructose and mannose, glycerophospholipid, taurine and hypotaurine, glycine, serine and threonine pathways. In rO and chRCC Glucosamine from amino sugar and nucleotide sugar metabolism pathway was dominantly abundant. Amino sugar and nucleotide sugar, glycerophospholipid and glutathione pathways are enriched in ccRCC. Sato et al. aimed to identify metabolites associated with early diagnosis and clinicopathological factors in RCC using global metabolomics (G-Met). Therefore, they analyzed 20 cases of ccRCC [19]. The results overlap with ours in several pathways, for example, the glycerophospholipid and gluthation pathways for ccRCC diagnosis, as well as the nucleotide sugar pathway for malignant status. For example, Glycerophospholipid is a glycerol-based phospholipid, which is a main component of biological membranes. Cancer cells undertake energy production in several ways. On the one hand via aerobic glycolysis, on the other hand via fatty acid oxidation. Furthermore, they produce Adenosintriphosphate (ATP) by catabolizing biological membranes [20]. Therefore, the decrease of glycerophospholipids could depend on the lipid catabolism to produce ATP from biological membranes [19].

The Gluthation pathway is another interesting pathway, which is enriched in different types of RCC. Glutathion is a tripeptide thiol antioxidant which contains the following amino acids: glutamic acid, cysteine, and glycine [21]. The main function of Gluthation is ROS scavenger in cells. Beside it, Glutathion is inter alia involved in the maturation of iron–sulfur proteins and detoxifying xenobiotics, as well as regulating redox signaling [22-24]. Hakimi et al. demonstrated that Gluthation metabolism-related metabolites, such as cysteine or γ-glutamyl cysteine, as well as Gluthation, have all been shown increased in late-stage ccRCC [25]. Furthermore, they are associated with worse survival outcomes in ccRCC patients. Alahmad et al. suggested that the metabolome showed an increase of reduced and oxidized Gluthation levels in pRCC [26]. In chRCC Xiao et al. and Priolo et al. detected an increase of Gluthation levels[27, 28]. An increased level of Gluthation was also detected in the benign rO by Kurschner et al. and Gopal et al.[29, 30].

These findings suggest that the Gluthation pathway plays an essential role in all primary renal tumors, malignant and benign ones. Therefore, it could be a suitable diagnostic for primary renal tumors in general but not for renal tumor subtyping. In comparison with the studies mentioned above, our results detected an increased Gluthation pathway only in ccRCC. An explanation for the lacking detection in the other subtypes could be the limited number of cases. In contrast to our study, Steurer et al. detected only moderate differences of detectable MALDI-MSI signals among the different histological tumor types including the ccRCC, the pRCC and the chRCC [7]. The cohort included 528

ccRCC, 41 chRCC and 112 pRCC. The collective is comparable with our cohort regarding the number of cases with the exception of chRCC. Steurer et al. detected two signals (m/z 1529.6 and 2056.2) that occurred significantly less frequently in ccRCC compared to pRCC. Between ccRCC or pRCC and chRCC no significant differences could be found. This fact could be explained by the small number of chRCC cases. In contrast to Steurer et al., Kriegsmann et al. achieved an overall accuracy of 89% by MSI for the classification between chRCC and rO. Kriegsmann et al. defined six most important markers (m/z 1377.6, m/z 1906.9, m/z 1786.8, m/z 1692.8, m/z 1629.8 and m/z 1495.7) for differential classification of chRCC and rO [8].

Niziol et al. analyzed urine samples from 50 patients with kidney cancer and 50 healthy volunteers using high-resolution proton nuclear magnetic resonance spectroscopy (^{1}H NMR) and silver-109 nanoparticle enhanced steel target laser desorption/ionization mass spectrometry (^{109}AgNPET LDI MS). The cohort included inter alia 33 ccRCC, 4 rO, 2 chRCC and 2pRCC. They identified twelve potential urine biomarkers of RCC [31]. Furthermore, Niziol et al. analyzed the metabolic pathways using MetaboAnalyst platform. They demonstrated four important pathways, which are related with the metabolic disturbances in patients with kidney cancer: including galactose, glycine, serine and threonine metabolism, tyrosine metabolism and aminoacyl-tRNA biosynthesis. You can find some overlaps here with our results. For example, we also detected an enriched pathway of the glycine, serin and threonine metabolism in the rO and the chRCC. This raises the question if these pathways play an essential role in oncocytic tumors. Exactly for these tumor subtypes novel diagnostic biomarker can improve the decision making. This pathway seems to play also a role in other urogenital carcinomas, for example in bladder cancer. Kouznetsova et al. explored that the glycine, serin and threonine metabolism is related to late-stage bladder cancer [32]. Further investigations should concentrate on this metabolism pathway in RCC studies.

Interestingly, our study showed beside pathway overlaps also metabolite overlaps between rO and chRCC, for example, Glucosamine. This fact supports the hypothesis, that both tumors originate from the same cell origin, that is, the intercalated cells of the collecting duct [33] . ccRCC and the pRCC originate both from the proximal tubules and also demonstrated common metabolites, e.g. 3-dehyrocarnitine.

Of course, our study shows several limitations: the relatively low number of cases, the use of TMAs, as well as the retrospective analysis. Furthermore, the use of MALDI-MSI is not suitable for routine diagnostic regarding the amount of time and availability.

Up to now, the data situation regarding the metabolic status is insufficient for all RCC subtypes. Especially studies which include smaller subgroups, such as chRCC and rO, are needed. Our results showed a mean accuracy in tumor discrimination of 85,13%. Moreover, several metabolic pathways were defined, which are enriched in special tumor subtypes.

Statement of Ethics

The study was approved by the Cantonal Ethics Committee of Zurich (BASEC-No_2019-01959) and the Ethics Committee of the Technical University of Munich (384/13) in accordance with the Swiss/German Human Research Act and with the Declaration of Helsinki. Informed written consent was assessed prior to intervention. Details that disclose the identity of the subjects under study were omitted.

Conflict of Interest Statement

The authors have declared no conflicts of interest.

Funding Sources

Author Contributions

Franziska Erlmeier, Na Sun, Arndt Hartmann and Axel Walch participated in the data interpretation and drafting of the manuscript. Na Sun and Jian Shen performed the statistical analysis. Franziska Erlmeier, Holger Moch and Peter Schraml carried out pathological data acquisition. Franziska Erlmeier and Peter Schraml provided the tissue micro arrays. Na Sun and Jian Shen carried out the MALDI analysis. Franziska Erlmeier, Na Sun, Jian Shen, Annette Feuchtinger, Achim Buck, Verena M. Prade, Thomas Kunzke, Peter Schraml, Holger Moch, Michael Autenrieth, Wilko Weichert, Arndt Hartmann and Axel Walch contributed to data interpretation and revised the manuscript for important intellectual content. All authors read and approved the final manuscript.

Data Availability Statement

All data generated or analysed during this study are included in this article. Further enquiries can be directed to the corresponding author.

REFERENCES

1.   Moch H, Cubilla AL, Humphrey PA, Reuter VE, Ulbright TM. The 2016 WHO Classification of Tumours of the Urinary System and Male Genital Organs-Part A: Renal, Penile, and Testicular Tumours. Eur Urol. 2016 Jul;70(1):93-105.

2.   Ljungberg B, Albiges L, Abu-Ghanem Y, Bensalah K, Dabestani S, Fernandez-Pello S, et al. European Association of Urology Guidelines on Renal Cell Carcinoma: The 2019 Update. Eur Urol. 2019 May;75(5):799-810.

3.   Amin MB, Paner GP, Alvarado-Cabrero I, Young AN, Stricker HJ, Lyles RH, et al. Chromophobe renal cell carcinoma: histomorphologic characteristics and evaluation of conventional pathologic prognostic parameters in 145 cases. Am J Surg Pathol. 2008 Dec;32(12):1822-34.

4.   Williamson SR, Gadde R, Trpkov K, Hirsch MS, Srigley JR, Reuter VE, et al. Diagnostic criteria for oncocytic renal neoplasms: a survey of urologic pathologists. Hum Pathol. 2017 May;63:149-56.

5.   Amin MB, Crotty TB, Tickoo SK, Farrow GM. Renal oncocytoma: a reappraisal of morphologic features with clinicopathologic findings in 80 cases. Am J Surg Pathol. 1997 Jan;21(1):1-12.

6.   Hes O, Michal M, Sima R, Vanecek T, Brunelli M, Martignoni G, et al. Renal oncocytoma with and without intravascular extension into the branches of renal vein have the same morphological, immunohistochemical and genetic features. Virchows Arch. 2008 Mar;452(3):285-93.

7.   Steurer S, Seddiqi AS, Singer JM, Bahar AS, Eichelberg C, Rink M, et al. MALDI imaging on tissue microarrays identifies molecular features associated with renal cell cancer phenotype. Anticancer Res. 2014 May;34(5):2255-61.

8.   Kriegsmann M, Casadonte R, Maurer N, Stoehr C, Erlmeier F, Moch H, et al. Mass Spectrometry Imaging Differentiates Chromophobe Renal Cell Carcinoma and Renal Oncocytoma with High Accuracy. J Cancer. 2020;11(20):6081-89.

9.   Erlmeier F, Hartmann A, Autenrieth M, Wiedemann M, Ivanyi P, Steffens S, et al. PD-1/PD-L1 expression in chromophobe renal cell carcinoma: An immunological exception? Med Oncol. 2016 Nov;33(11):120.

10.   Ly A, Buck A, Balluff B, Sun N, Gorzolka K, Feuchtinger A, et al. High-mass-resolution MALDI mass spectrometry imaging of metabolites from formalin-fixed paraffin-embedded tissue. Nat Protoc. 2016 Aug;11(8):1428-43.

11.   Wishart DS, Feunang YD, Marcu A, Guo AC, Liang K, Vazquez-Fresno R, et al. HMDB 4.0: the human metabolome database for 2018. Nucleic Acids Res. 2018 Jan 4;46(D1):D608-D17.

12.   Palmer A, Phapale P, Chernyavsky I, Lavigne R, Fay D, Tarasov A, et al. FDR-controlled metabolite annotation for high-resolution imaging mass spectrometry. Nat Methods. 2017 Jan;14(1):57-60.

13.   Chong J, Soufan O, Li C, Caraus I, Li S, Bourque G, et al. MetaboAnalyst 4.0: towards more transparent and integrative metabolomics analysis. Nucleic Acids Res. 2018 Jul 2;46(W1):W486-W94.

14.   Kanehisa M, Goto S. KEGG: kyoto encyclopedia of genes and genomes. Nucleic Acids Res. 2000 Jan 1;28(1):27-30.

15.   Zhang J, Li SQ, Lin JQ, Yu W, Eberlin LS. Mass Spectrometry Imaging Enables Discrimination of Renal Oncocytoma from Renal Cell Cancer Subtypes and Normal Kidney Tissues. Cancer Res. 2020 Feb 15;80(4):689-98.

16.   Eggleston LV, Krebs HA. Regulation of the pentose phosphate cycle. Biochem J. 1974 Mar;138(3):425-35.

17.   Riganti C, Gazzano E, Polimeni M, Aldieri E, Ghigo D. The pentose phosphate pathway: an antioxidant defense and a crossroad in tumor cell fate. Free Radic Biol Med. 2012 Aug 1;53(3):421-36.

18.   Lucarelli G, Galleggiante V, Rutigliano M, Sanguedolce F, Cagiano S, Bufo P, et al. Metabolomic profile of glycolysis and the pentose phosphate pathway identifies the central role of glucose-6-phosphate dehydrogenase in clear cell-renal cell carcinoma. Oncotarget. 2015 May 30;6(15):13371-86.

19.   Sato T, Kawasaki Y, Maekawa M, Takasaki S, Saigusa D, Ota H, et al. Value of global metabolomics in association with diagnosis and clinicopathological factors of renal cell carcinoma. Int J Cancer. 2019 Jul 15;145(2):484-93.

20.   Zira AN, Theocharis SE, Mitropoulos D, Migdalis V, Mikros E. (1)H NMR metabonomic analysis in renal cell carcinoma: a possible diagnostic tool. J Proteome Res. 2010 Aug 6;9(8):4038-44.

21.   Meister A. On the discovery of glutathione. Trends Biochem Sci. 1988 May;13(5):185-8.

22.   Awasthi YC, Misra G, Rassin DK, Srivastava SK. Detoxification of xenobiotics by glutathione S-transferases in erythrocytes: the transport of the conjugate of glutathione and 1-chloro-2,4-dinitrobenzene. Br J Haematol. 1983 Nov;55(3):419-25.

23.   Sipos K, Lange H, Fekete Z, Ullmann P, Lill R, Kispal G. Maturation of cytosolic iron-sulfur proteins requires glutathione. J Biol Chem. 2002 Jul 26;277(30):26944-9.

24.   Ren X, Zou L, Zhang X, Branco V, Wang J, Carvalho C, et al. Redox Signaling Mediated by Thioredoxin and Glutathione Systems in the Central Nervous System. Antioxid Redox Signal. 2017 Nov 1;27(13):989-1010.

25.   Hakimi AA, Reznik E, Lee CH, Creighton CJ, Brannon AR, Luna A, et al. An Integrated Metabolic Atlas of Clear Cell Renal Cell Carcinoma. Cancer Cell. 2016 Jan 11;29(1):104-16.

26.   Al Ahmad A, Paffrath V, Clima R, Busch JF, Rabien A, Kilic E, et al. Papillary Renal Cell Carcinomas Rewire Glutathione Metabolism and Are Deficient in Both Anabolic Glucose Synthesis and Oxidative Phosphorylation. Cancers (Basel). 2019 Sep 3;11(9).

27.   Priolo C, Khabibullin D, Reznik E, Filippakis H, Ogorek B, Kavanagh TR, et al. Impairment of gamma-glutamyl transferase 1 activity in the metabolic pathogenesis of chromophobe renal cell carcinoma. Proc Natl Acad Sci U S A. 2018 Jul 3;115(27):E6274-E82.

28.   Xiao YC, R.; Busch, J.F.; Rabien, A.; Kilic, E.; Villegas, S.; Türkmen, S.; Timmermann, B.; Attimonelli, M.; Jung, K.; et al. . Metabolic reprogramming and elevation of glutathione in chromophobe renal cell carcinomas. bioRxiv 2019.

29.   Kurschner G, Zhang Q, Clima R, Xiao Y, Busch JF, Kilic E, et al. Renal oncocytoma characterized by the defective complex I of the respiratory chain boosts the synthesis of the ROS scavenger glutathione. Oncotarget. 2017 Dec 1;8(62):105882-904.

30.   Gopal RK, Calvo SE, Shih AR, Chaves FL, McGuone D, Mick E, et al. Early loss of mitochondrial complex I and rewiring of glutathione metabolism in renal oncocytoma. Proc Natl Acad Sci U S A. 2018 Jul 3;115(27):E6283-E90.

31.   Niziol J, Ossolinski K, Tripet BP, Copie V, Arendowski A, Ruman T. Nuclear magnetic resonance and surface-assisted laser desorption/ionization mass spectrometry-based metabolome profiling of urine samples from kidney cancer patients. J Pharm Biomed Anal. 2021 Jan 30;193:113752.

32.   Kouznetsova VL, Kim E, Romm EL, Zhu A, Tsigelny IF. Recognition of early and late stages of bladder cancer using metabolites and machine learning. Metabolomics. 2019 Jun 20;15(7):94.

33.   Wobker SE, Williamson SR. Modern Pathologic Diagnosis of Renal Oncocytoma. J Kidney Cancer VHL. 2017;4(4):1-12.

FIGURES

Figure 1: Workflow of the MALDI-MSI analysis.

Figure 2: Pathway enrichment analysis of renal tumor subtypes with distinct metabolic profiles.

Figure 3: Example ion images of the discriminative metabolites. A. Ribose 5-phosphate, B. glucosamine, C. Uridine 5'-diphosphate. D. 3-Dehyrocarnitine. Each column indicates mean with standard error. P values are corresponding to the Kruskal–Wallis test.
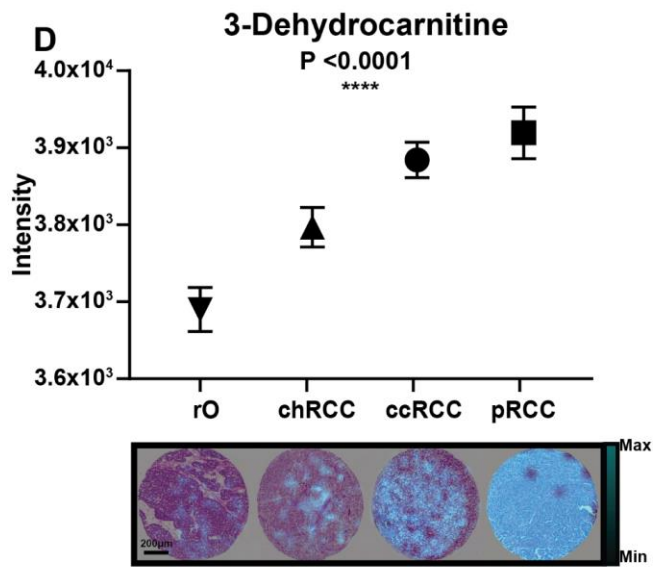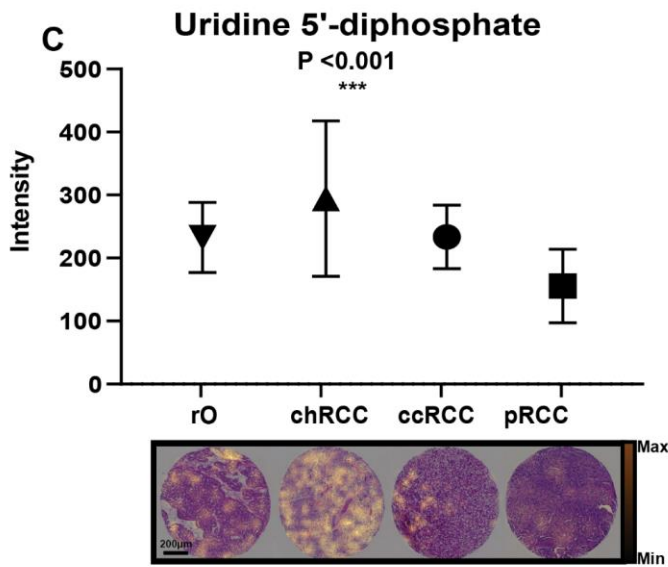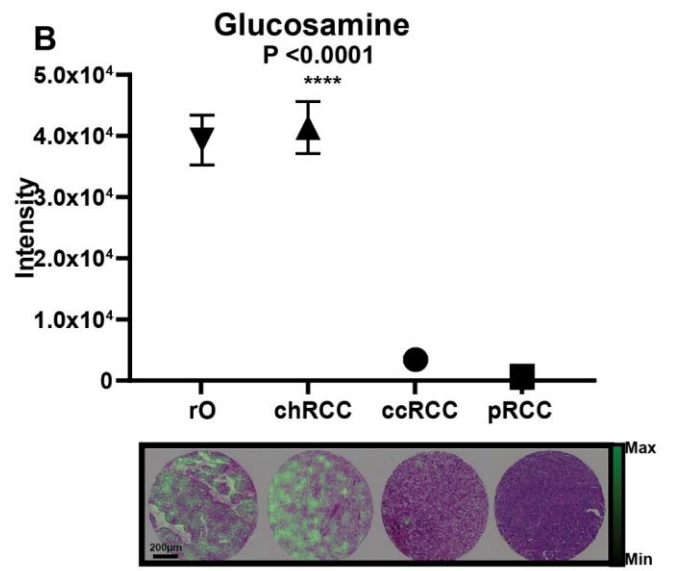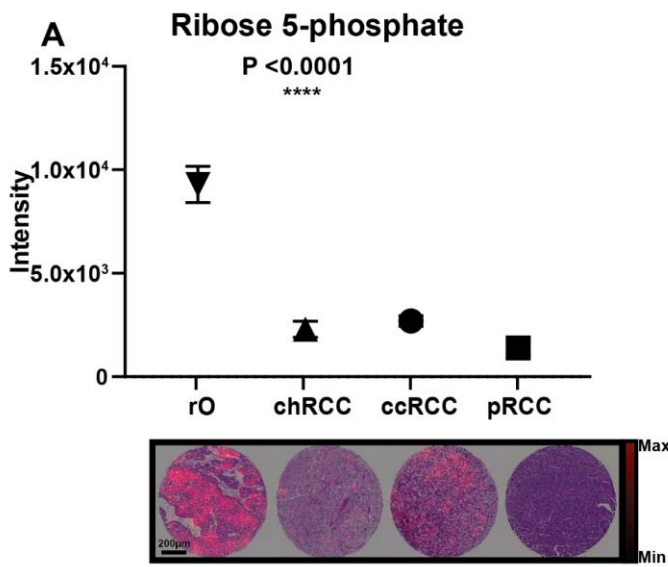
Workflow of MALDI and SPACiAL pipeline

A **Ribose 5-phosphate**
P <0.0001
****

B **Glucosamine**
P <0.0001
****

C **Uridine 5'-diphosphate**
P <0.001
***

D **3-Dehydrocarnitine**
P <0.0001
****
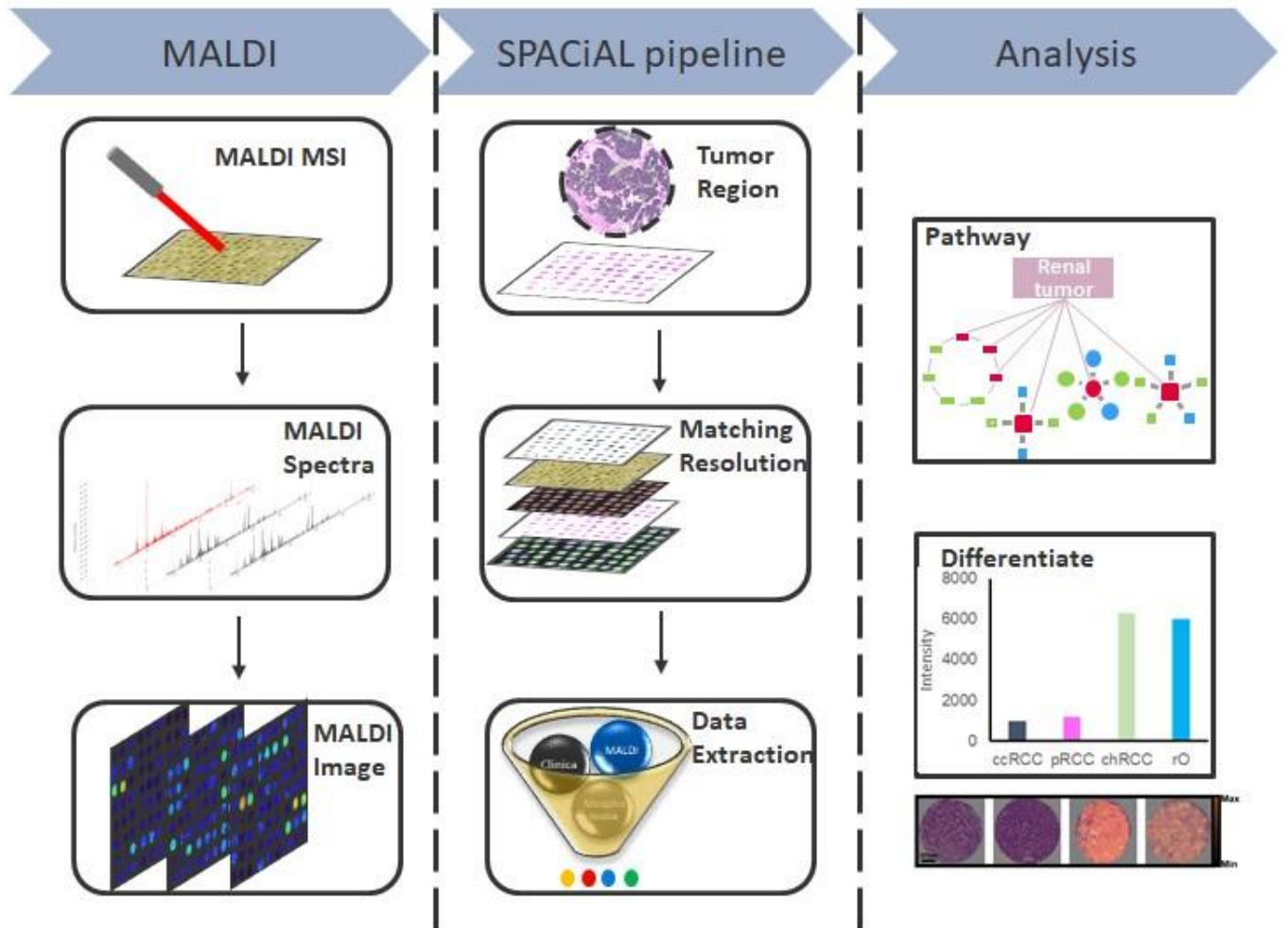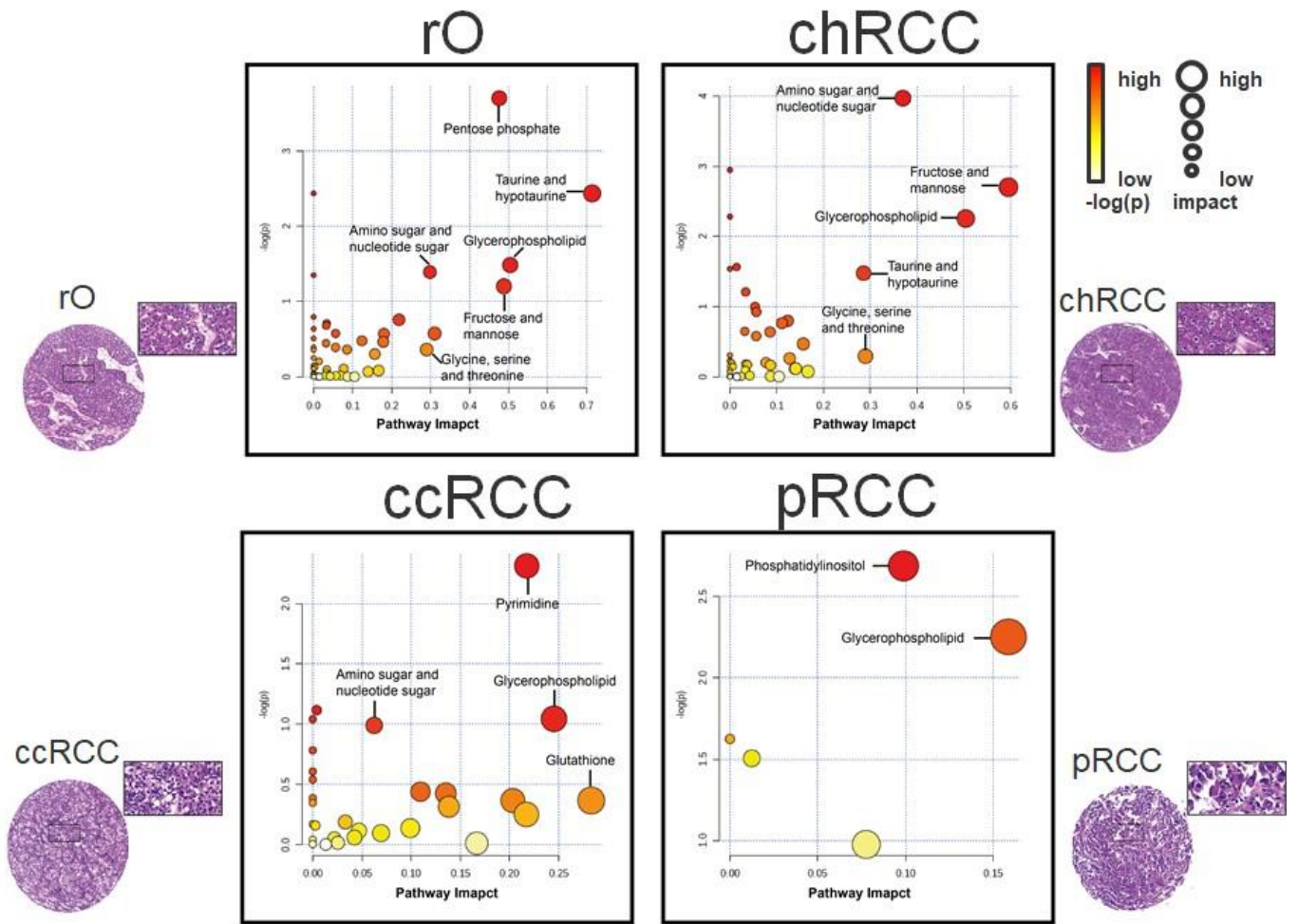
Table 1: Clinical and pathological characteristics. na = not available.

Patient characteristics	n = 853
Age median(range)(years)	27-88(65)
Gender	
Male	299
Female	441
na	113
ISUP Grade	
Grade 1	25
Grade 2	241
Grade 3	191
Grade 4	154
na	242
Pathological stage	
pT1	418
pT2	90
pT3	231
pT4	10
na	104
pN+	26
pM+	4
Subtype	
r0	71
chRCC	108
ccRCC	552
pRCC	122